https://doi.org/
https://orcid.org/

VILNIUS UNIVERSITY

Rokas
ASTRAUSKAS

Computer Modelling of Reaction-Diffusion Processes in Scanning Electrochemical Microscopy and in Cell Spheroids

DOCTORAL DISSERTATION

Natural Sciences,
Informatics (N 009)

VILNIUS 2021

This dissertation was written between 2014 and 2018 at Vilnius University.

Academic supervisor:
Prof. Dr. ... (Vilnius University, Natural Sciences, Informatics – N 009).

Dissertation Defence Panel:
Chair – **Prof. Dr. ...** (Vilnius University, Natural Sciences, Informatics – N 009).
Members:
Prof. ... (..., Natural Sciences, Informatics – N 009).
Prof. Dr. ... (..., Natural Sciences, Informatics – N 009).
Prof. Habil. Dr. ... (..., Natural Sciences, Informatics – N 009).
Dr. ... (Tallinn University of Technology, Estonia, Natural Sciences, Chemistry – N 003).

The dissertation shall be defended at a public meeting of the Dissertation Defence Panel at 10 a.m. on 6th October 2021 at the Institute of Computer Science of Vilnius University. Address: Didlaukio str. 47, LT-08303, Vilnius, Lithuania, tel. +370 5 219 5000; e-mail: mif@mif.vu.lt

The text of this dissertation can be accessed at the Library of Vilnius University and on the website of Vilnius University:
www.vu.lt/lt/naujienos/ivykiu-kalendorius.

https://doi.org/
https://orcid.org/

VILNIAUS UNIVERSITETAS

Rokas
ASTRAUSKAS

Reakcijos-difuzijos procesų kompiuterinis modeliavimas elektrocheminėje mikroskopijoje ir ląstelių sferoiduose

DAKTARO DISERTACIJA

Gamtos mokslai,
informatika (N 009)

VILNIUS 2021

Disertacija rengta 2014 – 2018 metais Vilniaus universitete.

Mokslinis vadovas:
prof. dr. ... (Vilniaus universitetas, gamtos mokslai, informatika – N 009).

Gynimo taryba:
Pirmininkė – **prof. dr. ...** (Vilniaus universitetas, gamtos mokslai, informatika – N 009).
Nariai:
prof. habil. dr. ... (..., gamtos mokslai, informatika – N 009).
prof. dr. ... (..., gamtos mokslai, informatika – N 009.)
prof. ... (..., gamtos mokslai, informatika - N 009).
dr. ... (Talino technikos universitetas, Estija, gamtos mokslai, chemija – N 003).

Disertacija ginama viešame Gynimo tarybos posėdyje 2021 m. spalio 6 d. 10 val. Vilniaus universiteto Matematikos ir informatikos fakulteto Informatikos instituto 211 auditorijoje. Adresas: Didlaulio g. 47, LT-08303, Vilnius, Lietuva, tel. +370 5 219 5000; el. paštas: mif@mif.vu.lt.

Disertaciją galima peržiūrėti Vilniaus universiteto bibliotekoje ir Vilniaus universiteto interneto svetainėje adresu: www.vu.lt/lt/naujienos/ivykiu-kalendorius.

Table of Contents

Introduction

Research area

The study is focused on computer modelling of complex chemical and biophysical systems, which are described by partial differential equations (PDEs) with nonlinear boundary conditions and PDEs in various complex (non-rectangular) domains. These differential problems are solved using numerical methods.

Problems of solving PDEs with nonlinear boundary conditions arise from mathematical modelling of complex chemical and biological processes in scanning electrochemical microscopy (SECM). The study of PDE in non-rectangular domains is motivated by the demand to estimate measurement errors due to deviations of SECM equipment geometry from the standard. Nonlinear systems of PDE are applied in the study of chemotherapeutic drugs uptake into tissues.

Actuality

...

Chapter 1

Modelling of SECM

1.1 Introduction

In the first chapter, the mathematical model of scanning electrochemical microscopy (SECM) redox-competition (RC-SECM) mode is presented for the first time in scientific research. The study is focused on solving systems of partial differential equations (PDEs) with nonlinear boundary conditions using numerical methods. Using this model, it is possible to calculate oxygen consumption rate, evaluate enzymatic reaction kinetics and determine oxygen diffusion coefficients in the medium of varying composition. Oxygen concentration measurement, which is important for SECM-based investigations of all biological systems, was successfully applied for the evaluation of enzymatic reaction performed by an immobilized enzyme.

Scanning electrochemical microscopy

Scanning electrochemical microscopy is an advanced electrochemical method, which is based on electrochemical measurements with the scanning ultramicroelectrode (UME). In this approach, the UME, which has the diameter of conducting part in the range of several tenths of micrometres and insulator part of few hundreds of micrometres, is scanning 3D space close to catalytic or electrochemically active surfaces [1]. In such an experiment the UME is connected as a working electrode in an electrochemical cell, and the current, which is measured by the UME, depends on the local concentration of electroactive species.

Electron transfer kinetics of surfaces modified by enzymes is mostly investigated using feedback (FB) or generation-collection modes of SECM [4, 10, 11, 13]. In addition, SECM was applied for high-resolution imaging of the chemical reactivity [12, 14], electrocatalytic activity [5, 7, 16], and topography of enzyme-based interfaces formed in enzyme immunoassays [15], biosensors and biochips [17].

1.2 Physical model

Reaction rate constants

In this research, the kinetic constants for reactions were gathered from references [2, 6, 9] and adjusted to better fit experimental results (Table 1.1). Kinetic constants k_{-1}, k_{-3}, k_{-4} for reactions were determined from the model and were set to the following values: $k_{-1} = 10\,\mathrm{s}^{-1}$, $k_{-3} = 2000\,\mathrm{M}^{-1}\mathrm{s}^{-1}$. The constant k_{-4} was set to zero, because the backward reaction is much slower than other reactions in diffusion-related processes.

Table 1.1: Kinetic constants and thermodynamic parameters for the GOx catalyzed reaction with β-D-glucose and oxygen at pH 5.5.

Sugar substrate or thermodynamic parameter	k_1, $\mathrm{M}^{-1}\mathrm{s}^{-1}$	k_2, s^{-1}	k_3, $\mathrm{M}^{-1}\mathrm{s}^{-1}$	k_4, s^{-1}	ref.
β-D-glucose-1-^{1}H at 25 °C	∼200	∼6000	1.8×10^6	1440	[9]
β-D-glucose-1-^{1}H at 25 °C	13 158		1.8×10^6	1440	[2]
β-D-glucose-1-^{1}H at 27 °C	10 000		2.1×10^6	1150	[6]
Used in the model	3000	6000	1.5×10^6	1500	

1.3 Mathematical model

Measurements of SECM acting in the redox-competition mode are changed into the scheme (1.1) due to the radial symmetry around the

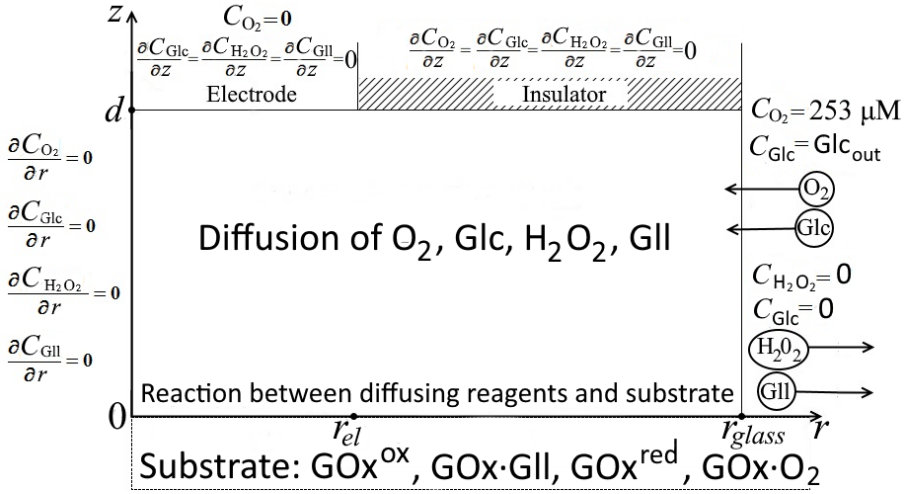

Figure 1.1: Scheme of simulation domain. All 8 reagents, boundary conditions for C_{diff} and the direction of outside flux are displayed.

central axis of the electrode. Radial symmetry is a standard assumption in SECM modelling, though the case of off-centered UME was also investigated [3].

According to the second Fick's law [8], diffusion processes are expressed by the system of partial differential equations (PDE):

$$\begin{aligned}
\frac{\partial C_{O_2}}{\partial t} &= D_{O_2}\,\Delta C_{O_2},\\
\frac{\partial C_{Glc}}{\partial t} &= D_{Glc}\,\Delta C_{Glc},\\
\frac{\partial C_{H_2O_2}}{\partial t} &= D_{H_2O_2}\,\Delta C_{H_2O_2},\\
\frac{\partial C_{Gll}}{\partial t} &= D_{Gll}\,\Delta C_{Gll}, \quad for\ 0<t\le T,\ 0<z<d,\ 0<r<r_{glass},
\end{aligned} \tag{1.1}$$

where:

C_{O_2}, C_{Glc}, $C_{H_2O_2}$ and C_{Gll} are concentrations of diffusing reagents and expressed as functions of time t and spatial coordinates z and r. Notation $C_{\text{diff}} = C_{\text{diff}}(t,z,r) = (C_{O_2}, C_{Glc}, C_{H_2O_2}, C_{Gll})$ was used when 4 diffusing reagents were considered together.

D_{O_2}, D_{Glc}, $D_{H_2O_2}$ and D_{Gll} are diffusion coefficients of O_2, Glc, H_2O_2 and Gll.

d is the distance between the enzyme-modified surface and the electrode, which is varying from $1\,\mu\mathrm{m}$ to $120\,\mu\mathrm{m}$ as shown in Fig. 1.1.

$r_{glass} = 80\,\mu\mathrm{m}$ is the radius of insulated area, $r_{el} = 5\,\mu\mathrm{m}$ is the radius of electrode.

T is the duration of a computational experiment measured in seconds (the evaluation of this parameter is further explained in the next section).

The Laplace operator Δ for concentration function C in cylindrical coordinates with radial symmetry is

$$\Delta C = \frac{1}{r}\frac{\partial}{\partial r}\left(r\frac{\partial C}{\partial r}\right) + \frac{\partial^2 C}{\partial z^2}.$$

Conclusions

...

Bibliography

[1] A. J. Bard, F. R. F. Fan, J. Kwak, and O. Lev. Scanning electrochemical microscopy. Introduction and principles. *Analytical Chemistry*, 61(2):132–138, 1989.

[2] H. J. Bright and Q. H. Gibson. The oxidation of 1-deuterated glucose by glucose oxidase. *Journal of Biological Chemistry*, 242(5):994–1003, 1967.

[3] R. Cornut, A. Bhasin, S. Lhenry, M. Etienne, and C. Lefrou. Accurate and simplified consideration of the probe geometrical defaults in scanning electrochemical microscopy: Theoretical and experimental investigations. *Analytical Chemistry*, 83(24):9669–9675, 2011. doi: 10.1021/ac2026018.

[4] S. A. G. Evans, K. Brakha, M. Billon, P. Mailley, and G. Denuault. Scanning electrochemical microscopy (SECM): localized glucose oxidase immobilization via the direct electrochemical microspotting of polypyrrole–biotin films. *Electrochemistry Communications*, 7 (2):135–140, 2005.

[5] J. L. Fernandez and A. J. Bard. Scanning electrochemical microscopy. 47. Imaging electrocatalytic activity for oxygen reduction in an acidic medium by the tip generation-substrate collection mode. *Analytical Chemistry*, 75(13):2967–2974, 2003.

[6] Q. H. Gibson, B. E. P. Swoboda, and V. Massey. Kinetics and mechanism of action of glucose oxidase. *Journal of Biological Chemistry*, 239(11):3927–3934, 1964.

[7] L. Guadagnini, A. Maljusch, X. Chen, S. Neugebauer, D. Tonelli, and W. Schuhmann. Visualization of electrocatalytic activity of microstructured metal hexacyanoferrates by means of redox competition mode of scanning electrochemical microscopy (RC-SECM). *Electrochimica Acta*, 54(14):3753–3758, 2009.

[8] F. O. Laforge, P. Sun, and M. V. Mirkin. Physicochemical applications of scanning electrochemical microscopy. *Advances in Chemical Physics*, 139:177–244, 2008.

[9] V. Leskovac, S. Trivić, G. Wohlfahrt, J. Kandrač, and D. Peričin. Glucose oxidase from *Aspergillus niger*: the mechanism of action

with molecular oxygen, quinones, and one-electron acceptors. *The International Journal of Biochemistry & Cell Biology*, 37(4):731–750, 2005.

[10] I. Morkvenaite-Vilkonciene, P. Genys, A. Ramanaviciene, and A. Ramanavicius. Scanning electrochemical impedance microscopy for investigation of glucose oxidase catalyzed reaction. *Colloids and Surfaces B: Biointerfaces*, 126:598–602, 2015.

[11] D. T. Pierce, P. R. Unwin, and A. J. Bard. Scanning electrochemical microscopy. 17. Studies of enzyme-mediator kinetics for membrane- and surface-immobilized glucose oxidase. *Analytical Chemistry*, 64 (17):1795–1804, 1992.

[12] R. Teranishi, E. Higuchi, M. Chiku, and H. Inoue. Analysis of kinetics of oxygen reduction reaction in alkaline solution by scanning electrochemical microscopy. *Ecs Transactions*, 41(1):2179–2184, 2011.

[13] T. Wilhelm and G. Wittstock. Analysis of interaction in patterned multienzyme layers by using scanning electrochemical microscopy. *Angewandte Chemie International Edition*, 42(20):2248–2250, 2003.

[14] G. Wittstock, M. Burchardt, S. E. Pust, Y. Shen, and C. Zhao. Scanning electrochemical microscopy for direct imaging of reaction rates. *Angewandte Chemie International Edition*, 46(10):1584–1617, 2007.

[15] T. Yasukawa, Y. Hirano, N. Motochi, H. Shiku, and T. Matsue. Enzyme immunosensing of pepsinogens 1 and 2 by scanning electrochemical microscopy. *Biosensors and Bioelectronics*, 22(12):3099–3104, 2007.

[16] H. Ye, H. S. Park, and A. J. Bard. Screening of electrocatalysts for photoelectrochemical water oxidation on W-doped $BiVO_4$ photocatalysts by scanning electrochemical microscopy. *The Journal of Physical Chemistry C*, 115(25):12464–12470, 2011.

[17] C. Zhao and G. Wittstock. Scanning electrochemical microscopy for detection of biosensor and biochip surfaces with immobilized pyrroloquinoline quinone (PQQ)-dependent glucose dehydrogenase as enzyme label. *Biosensors and Bioelectronics*, 20(7):1277–1284, 2005.

Santrauka (Summary in Lithuanian)

Tyrimų sritis

Pasitelkus kompiuterinį modeliavimą disertacijoje tiriamos sudėtingos cheminės ir biofizikinės sistemos, kurios yra aprašomos dalinių išvestinių lygtimis (DIL) su netiesinėmis kraštinėmis sąlygomis ir DIL sudėtingos geometrijos (nestačiakampėse) srityse. Šios DIL sprendžiamos baigtinių skirtumų metodu ir kitais skaitiniais algoritmais.

DIL sprendimo su netiesinėmis kraštinėmis sąlygomis problemos kyla dėl cheminių ir biologinių procesų matematinio modeliavimo. Tyrimai nestačiakampėse srityse yra aktualūs dėl poreikio įvertinti matavimo prietaisų paklaidas, atsirandančias dėl geometrijos nukrypimo nuo standarto. DIL netiesinės sistemos yra pritaikytos tyrinėti chemoterapinių vaistų patekimą į audinius.

Tikslas

...

S.1 SECM modeliavimas oksidacijos-redukcijos konkurencijos režime

S.1.1 Matematinis modelis

Dėl simetrijos aplink centrinę elektrodo ašį modelis užrašomas cilindrinėse koordinatėse. Cilindro formos srityje atliekami SECM matavimai yra pakeisti į 2D sritį S.1 pav.

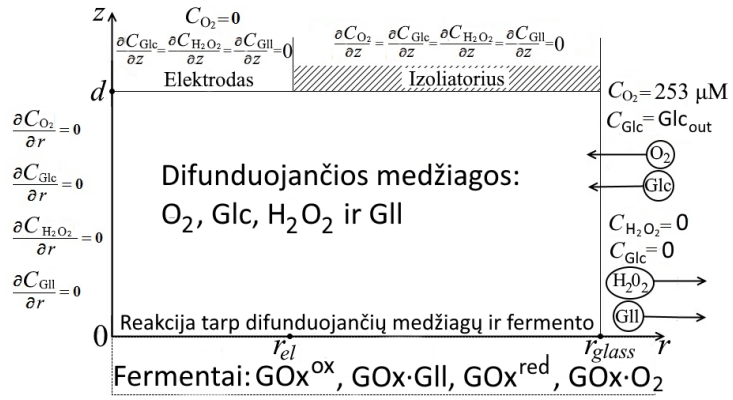

S.1 pav.: Modeliavimo srities schema. Pavaizduotos 8 modeliuotos medžiagos - 4 difunduojantys reagentai bei 4 fermento GOx formos, kraštinės sąlygos 4-ioms difunduojančioms medžiagoms ir išorinis srautas.

Difuzijos procesai išreiškiami antruoju Fiko dėsniu [8]:

$$\begin{aligned}
\frac{\partial C_{O_2}}{\partial t} &= D_{O_2}\,\Delta C_{O_2},\\
\frac{\partial C_{Glc}}{\partial t} &= D_{Glc}\,\Delta C_{Glc},\\
\frac{\partial C_{H_2O_2}}{\partial t} &= D_{H_2O_2}\,\Delta C_{H_2O_2},\\
\frac{\partial C_{Gll}}{\partial t} &= D_{Gll}\,\Delta C_{Gll}, \quad 0<t\le T,\ 0<z<d,\ 0<r<r_{glass}.
\end{aligned} \tag{S.1}$$

Šiose lygtyse:

C_{O_2}, C_{Glc}, $C_{H_2O_2}$ ir C_{Gll} yra atitinkamų difunduojančių reagentų koncentracijos, kurios išreiškiamos kaip laiko t, erdvinių koordinačių z ir r funkcijos.

D_{O_2}, D_{Glc}, $D_{H_2O_2}$ ir D_{Gll} yra difuzijos koeficientai.

d yra atstumas tarp fermentu modifikuoto paviršiaus ir elektrodo. Skaitinio eksperimento metu d keičiamas nuo $1\,\mu\mathrm{m}$ iki $120\,\mu\mathrm{m}$. Tai atitinka elektrodo stumdymą aukštyn ir žemyn cheminio eksperimento metu.

$r_{glass} = 80\,\mu\mathrm{m}$ yra izoliuotos srities spindulys.

T yra skaičiavimo eksperimento trukmė, matuojama sekundėmis.

Laplaso operatorius Δ cilindrinėse koordinatėse su centrine simetrija yra

$$\Delta C = \frac{1}{r}\frac{\partial C}{\partial r}\left(r\frac{\partial C}{\partial r}\right) + \frac{\partial^2 C}{\partial z^2}.$$

Curriculum Vitae

Rokas Astrauskas graduated from ...

Acknowledgements

Not required/Padėka neprivaloma

Rokas Astrauskas
Vilnius
21st October 2021

Publications by the Author

1st publication

Modeling the uptake of fluorescent molecules into 3D cellular spheroids

R. Astrauskas, F. Ivanauskas, G. Jarockytė, V. Karabanovas, and R. Rotomskis

Nonlinear Analysis: Modelling and Control, 24(5): 838–852, 2019

DOI: 10.15388/NA.2019.5.9

Nonlinear Analysis: Modelling and Control, Vol. 24, No. 5, 838–852
https://doi.org/10.15388/NA.2019.5.9

ISSN: 1392-5113
eISSN: 2335-8963

Modeling the uptake of fluorescent molecules into 3D cellular spheroids

Rokas Astrauskas[a], **Feliksas Ivanauskas**[a], **Greta Jarockytė**[b], **Vitalijus Karabanovas**[b,c], **Ričardas Rotomskis**[b,d]

[a]Institute of Computer Science, Faculty of Mathematics and Informatics, Vilnius University, Didlaukio str. 47, LT-08303 Vilnius, Lithuania
rokas.astrauskas@mif.vu.lt

[b]Laboratory of Biomedical Physics, National Cancer Institute, Baublio str. 3b, LT-08406 Vilnius, Lithuania

[c]Department of Chemistry and Bioengineering, Vilnius Gediminas Technical University, Saulėtekio ave. 11, LT-10223 Vilnius, Lithuania

[d]Biophotonics group of Laser Research Center, Faculty of Physics, Vilnius University, Saulėtekio str. 9, bldg. 3, LT-10222 Vilnius, Lithuania

Received: June 6, 2019 / **Revised:** September 2, 2019 / **Published online:** September 27, 2019

Abstract. Three mathematical models were developed to analyze the dynamics of fluorescent dyes penetration into 3D cellular spheroids. Two fluorescent dyes were chosen to verify mathematical models: rhodamine 6G (R6G) as a small molecule, which can freely penetrate through the cells, and wheat germ agglutinin (WGA) conjugated with Alexa488 fluorescent label, which reacts with the cells plasma membrane, and its cellular penetration is significantly lower. Dye penetration and binding to cells were modeled with nonlinear diffusion–reaction equations. System of differential equations was solved using numerical methods, and good correspondence with physical experiment was shown. Diffusion coefficients in extracellular matrix were determined for both fluorescent dyes, and the influence of reactions parameters to WGA penetration was analyzed. Dynamics of dyes accumulation into cell spheroids were also determined.

Keywords: diffusion reaction equations, cellular spheroids, rhodamine 6G, wheat germ agglutinin, mathematical modeling.

1 Introduction

Recently, the application of 3D cell cultures in various biomedical studies has emerged. It is agreed that this method is more relevant to native tissues than the former gold standard – cell monolayers. 3D cell cultures are usually used as a platform for primary drug testing, however, due to some limitations, not all drugs can be investigated. In that case, it would be useful to have mathematical models, which would predict drug accumulation and

© 2019 Authors. Published by Vilnius University Press
This is an Open Access article distributed under the terms of the Creative Commons Attribution Licence, which permits unrestricted use, distribution, and reproduction in any medium, provided the original author and source are credited.

distribution in 3D cell cultures by using the data of similar already investigated molecules. The fluorescent dyes, which physico-chemical characteristics such as structure and molecular mass are very similar to chemotherapeutic agents, could be used for modeling and quantification of drug penetration in 3D cell cultures.

One of the most commonly used 3D cell cultures are cellular spheroids. Cellular spheroids are self-assembled clusters of cell colonies cultured in environments, where cell–cell interactions dominate over cell–substrate interactions. Some authors have published their attempts to simulate how various nanoparticles (NPs) accumulate and distribute in cellular spheroids. Gao et al. have established and studied a computational model to predict the time- and concentration-dependent diffusion of NPs in tumor cellular spheroids [9]. The mathematical model of antibody penetration into tumor spheroids was developed to gain an improved understanding of the quantitative interplay among the rate processes of diffusion, binding, degradation, and plasma clearance [12]. The same model was used to describe the diffusion of NPs into multicellular spheroids in the presence of the extracellular matrix modulator, collagenase [11]. The results from the proposed model, in combination with the experimental results, suggested that particle size, particle binding, and porosity of biological tissue are the key parameters that need to be considered when designing NP drug carriers for cancer treatment. Our previous experimental study and modeling results also demonstrated that penetration of carboxylated nanoparticles was strongly limited and dependent on size and porosity of cellular spheroids [14].

Chariou et al. provided the model to quantify diffusion and uptake of tobacco mosaic virus (TMV) in a spheroid system approximating a capillary-free segment of a solid tumor [5]. Model simulations predicted TMV concentration distribution over time in a tumor spheroid for different sizes and cell densities.

Oxygen consumption and diffusion in cellular spheroids were analyzed, and a method was presented for estimating the rates of oxygen consumption and diffusion limit, the extents of the necrotic core, hypoxic region, and proliferating rim [13].

Uptake and inward diffusion of a fluorescent dye calcein via gap junction intercellular communication were studied using a 3D multilayer spheroid model [1]. Quantitative studies about the kinetic parameters for efflux of various rhodamine dyes were performed [18] but only for 2D cell cultures. As far as we know, there are no mathematical models, which would predict diffusion and accumulation of organic molecules (e.g., drugs or dyes) in 3D cell cultures.

Rhodamine 6G (R6G) is a fluorescent positively charged lipophilic dye, which specifically stains and selectively accumulates in mitochondria. It was also reported that at higher concentrations, R6G also stained endoplasmic reticulum and other membrane organelles. Due to its lipophilic nature, R6G is also known as a specific stain for detection of lipids. This allows R6G to be used as a universal lipid marker for both qualitative [7] and quantitative research [4]. Masuda and Oguma study showed that R6G dye could be used not only for *in vitro* cell studies but also for visualizing the vascular networks of the liver and to examine the intrahepatic flow distribution under various conditions [15].

Wheat germ agglutinin (WGA) is a lectin that protects wheat (*Triticum*) from insects, yeast, and bacteria. Wheat germ agglutinin selectively binds to N-acetylglucosamine and N-acetylneuraminic acid (sialic acid), residues which are predominantly found on

the plasma membrane [20]. WGA conjugated to Alexa Fluor fluorophores is used as a fluorescent marker to stain the plasma membrane of various mammalian cells.

In this study, a nonlinear system of diffusion–reaction equations was used for modeling the diffusion of WGA-Alexa488 and R6G as well as the binding of WGA-Alexa488 to the cells. Three different cases of the system were presented to describe the diffusion into cellular spheroids of these dyes. Laplace operator of the nonlinear system was written in spherical coordinates because the modeled area is a sphere. The system was solved using a finite difference method, and the resulting nonlinear system of algebraic equations was solved with an iterative method.

The computational results and the physical experiment were compared and close correspondence between them was achieved. Diffusion coefficients in the extracellular matrix for both dyes were calculated using model and experiment comparison. Moreover, the ratio between the dye concentration and the fluorescence intensity was evaluated. The influence of reaction parameters to dye penetration was analyzed. Dynamics of dyes uptake were estimated for spheroids of different size and cell/matrix density.

In Section 2, physical/biological experiment was explained. In Section 3, details about three mathematical models were presented alongside calculations of equations parameters. In Section 4, computational and physical experiments were compared, and results of the study are discussed.

2 Materials and methods

Cell culturing. Immortalized mouse embryonic fibroblast cell line NIH3T3 was used, which was purchased from American Type Culture Collection. Cells were cultured in cell growth medium (Dulbecco's Modified Eagle Medium – DMEM) supplemented with 10% (v/v) fetal bovine serum (FBS), 100 U/mL penicillin, and 100 μg/mL streptomycin (all from Gibco, US). Cells were maintained at $37\,^{\circ}$C in a humidified atmosphere containing 5% of CO_2. The cells were routinely subcultured $2-3$ times a week in 25 cm^2 culture dishes.

Cellular spheroids. Cellular spheroids were formed using the hanging drop technique, using a 96-well hanging drop plate Perfecta3D® (3D Biomatrix, USA). During the experiments, the initial number of cells in the drop was varied from 6000 to 16000 cells per drop. The plate was maintained at $37\,^{\circ}$C in a humidified atmosphere containing 5% of CO_2. To provide enough nutrients for the cells and to prevent an osmolality shift in the medium, 4 μL of a fresh cell growth medium were added daily to each well. Cellular spheroids were grown for 4 days before experiments.

Dyes used for modeling diffusion. Commercially available rhodamine 6G – R6G (Sigma Aldrich, Germany) dye was used for the investigation of small molecules penetration in cellular spheroids. To prepare an R6G stock solution, 1 mg of R6G powder was dissolved in 1 mL of phosphate buffered saline – PBS pH 7.4 (Gibco, UK). The stock solution was diluted with cell growth medium to the final concentration of 5 μg/mL (10.4 μM).

Wheat germ agglutinin (WGA) conjugated to Alexa Flour 488 (WGA-Alexa488, Thermo Fisher, US) was used as a model of a molecule, which reacts with the cell plasma membrane and cannot penetrate freely through the plasma membrane like small molecules such as R6G. WGA-Alexa488 working solutions were prepared as suggested in the manufacturer's protocol. The final concentration used for 3D cell cultures was $0.13\ \mu$M.

Imaging of R6G and WGA-Alexa488 distribution in cellular spheroids. The accumulation of R6G in cellular spheroids was observed using a confocal Nikon Eclipse Te2000-U C1 Plus Laser scanning microscope equipped with an argon laser for 488 nm excitation (Nikon, Japan). Imaging was performed using 20x/0.50 NA objective (Nikon, Japan). The three-channel RGB detector (band-pass filters 450/17, 515/15, and 605/35 for blue, green, and red channels, respectively) was used. Image processing was performed using the Nikon EZ-C1 Bronze version 3.80 and ImageJ 1.46 software.

Quantification of R6G accumulation in cellular spheroids. Cellular spheroids were formed as described earlier. After incubations with R6G, spheroids were transferred to 1.5 mL centrifuge tubes and suspended in 1 mL PBS, then centrifuged $200 \times$ g for 7 min to separate free R6G in media. The supernatant was removed and spheroids were dissociated with 0.25% trypsin for 10 min to dissociate cells. Then cell suspension was mixed with PBS and centrifuged $200 \times$ g for 7 min.

After centrifugation, all cell samples were resuspended in $50\ \mu$l PBS and analyzed with BD Accuri C6 flow cytometer (Accuri Cytometers, Inc., Ann Arbor, MI, USA). The data were analyzed with FlowJo software (Tree Star, Inc., Ashland, OR, USA).

3 Mathematical models

3.1 WGA migration modeled with diffusion–reaction equations

Diffusion is the driver of biological processes in cells and 3D spheroids. The diverse temporal scales of intracellular and intercellular processes are determined by vastly diverse spatial and temporal scales in most biological and biophysical processes.

WGA molecules diffusion and binding in 3D cell spheroids is expressed by the equation

$$\begin{aligned}\frac{\partial C_{\mathrm{out}}}{\partial t} &= D\frac{1}{r^2}\frac{\partial}{\partial r}\left(r^2\frac{\partial C_{\mathrm{out}}}{\partial r}\right)\\ &\quad - k_{\mathrm{bind}}(B_{\max} - C_{\mathrm{bind}})C_{\mathrm{out}}, \quad 0 < t \leqslant T,\ 0 < r < R,\end{aligned} \tag{1}$$

where k_{bind} is a rate constant of binding of WGA to the cells membrane, R is the radius of a spheroid, D – diffusion coefficient, $C_{\mathrm{out}}(t, r)$ is the concentration of WGA molecules in spheroid as a function on time and coordinate, t – time variable, r – the distance from the center of sphere, T – modeling duration.

Diffusion equation was written in spherical coordinates, and assumption was made that spheroids are approximately uniform in all directions.

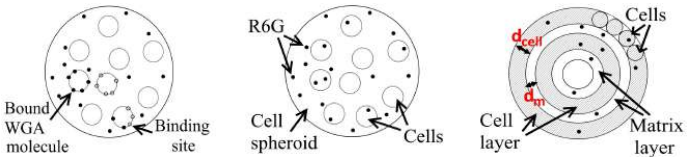

(a) (b) (c)

Figure 1. (a) WGA model, (b) R6G model, (c) rings model.

As shown in Fig. 1(a), there is a limited number of sites on cell membranes for molecules to bind, which is denoted by the constant $B_{\max}$ [8]. When this number is reached, no molecules can bind on the cell membrane. The process of binding to cells is modeled by the equation

$$\frac{\partial C_{\text{bind}}}{\partial t} = k_{\text{bind}}(B_{\max} - C_{\text{bind}})C_{\text{out}}, \quad 0 < t \leqslant T, \tag{2}$$

where $C_{\text{bind}}(t, r)$ is the concentration of WGA molecules, which are bound to the cells membrane.

Following boundary conditions are used:

$$C_{\text{out}}|_{r=R} = C_{\text{outside}}, \quad \left.\frac{\partial C_{\text{out}}}{\partial r}\right|_{r=0} = 0, \quad t > 0, \tag{3}$$

which show that in the exterior of a spheroid, there is a constant concentration of WGA molecules $C_{\text{outside}} = 5\ \mu\text{g/mL}/(38643\ \text{g/mol}) = 0.13\ \mu\text{M}$ (M = mol/L is molar concentration) and that there is symmetry to the center of a spheroid.

Initial conditions for both functions of concentrations are

$$C_{\text{out}}|_{t=0} = 0, \quad C_{\text{bind}}|_{t=0} = 0, \quad 0 \leqslant r \leqslant R, \tag{4}$$

indicating that there is no WGA molecules at the start of experiment and all binding sites are free.

3.2 Rhodamine migration modeled with diffusion equation

Rhodamine R6G diffuses both through cells and cellular matrix (Fig. 1(b)), and thus diffusion of R6G molecules in spheroids is modeled using the diffusion equation

$$\frac{\partial C}{\partial t} = D\frac{1}{r^2}\frac{\partial}{\partial r}\left(r^2\frac{\partial C}{\partial r}\right), \quad 0 < t \leqslant T,\ 0 < r < R, \tag{5}$$

where $C(t, r)$ is R6G concentration, and it is a version of (1) without the reaction element.

The same boundary conditions are used for R6G model as in (3):

$$C|_{r=R} = C_{\text{outside}}, \quad \left.\frac{\partial C}{\partial r}\right|_{r=0} = 0, \quad t > 0. \tag{6}$$

Molar concentration $C_{\text{outside}} = 5\ \mu\text{g/mL}/(493\ \text{g/mol}) = 10.4\ \mu\text{M}$ is greater for R6G due to a smaller molar mass than WGA-Alexa488.

Initially, there are no rhodamine molecules in spheroid, so we have

$$C|_{t=0} = 0, \quad 0 \leqslant r \leqslant R. \tag{7}$$

It should be noted that R6G model is separate linearized version of WGA model given by (1)–(4), but with k_{bind} set to 0 and different coefficients.

3.3 Rhodamine migration using rings of cells and matrix layers model

Spheroids were modeled as concentric rings of cells and matrix layers as in Fig. 1(c), where cell rings represent averaged cells, and cellular matrix layer – material between the cells. The process is expressed by equation

$$\frac{\partial C}{\partial t} = \frac{1}{r^2}\frac{\partial}{\partial r}\left(r^2 D(r)\frac{\partial C}{\partial r}\right), \quad 0 < t \leqslant T,\ 0 < r < R, \tag{8}$$

where $D(r)$ is a function representing diffusion coefficient,

$$D(r) = \begin{cases} D_{\text{cell}} & \text{if } r \in \text{cell layer}, \\ D_{\text{matrix}} & \text{if } r \in \text{matrix layer}. \end{cases}$$

D_{cell} is diffusion coefficient in cells, and D_{matrix} is diffusion coefficient in cellular matrix. $d_{\text{cell}} = 10\ \mu\text{m}$ is an average diameter of cells, and d_m is an average distance between cells, which was calculated in such a way that a known number of cells N of size d_{cell} would fit into the spheroid of radius R.

Boundary and initial conditions remain the same as in Section 3.2:

$$\begin{aligned} &C|_{r=R} = C_{\text{outside}}, \quad \left.\frac{\partial C}{\partial r}\right|_{r=0} = 0, \quad t > 0, \\ &C|_{t=0} = 0, \quad 0 \leqslant r \leqslant R. \end{aligned} \tag{9}$$

3.4 Calculation of coefficients and numerical solution

The R6G dye diffuses both through the cells at diffusion rate D_{cell} and the extracellular matrix at the rate D_{matrix}. In the study, diffusion coefficient for R6G model in (5) was averaged in the whole spheroid:

$$D = \phi D_{\text{cell}} + (1 - \phi) D_{\text{matrix}},$$

where $\phi = N_{\text{cell}}\, V_{\text{cell}}/V_{\text{sphere}}$ is the proportion of total cell volume to spheroid volume, $(1 - \phi)$ – the proportion of extracellular matrix volume to spheroid volume, V_{cell} is the volume of a cell, which is considered to be spherical, V_{sphere} – the volume of cellular spheroid. N_{cell} is the number of cells in particular spheroid ranging from 6000 to 14000.

The diffusion coefficient of R6G or similar rhodamine dyes was investigated theoretically and experimentally by many authors. It was observed that the coefficient varies from $4.0 \cdot 10^{-10}$ m^2/s in water solutions [10] to $1.5 \cdot 10^{-18}$ m^2/s in high concentration sucrose–water solutions [6]. $D_{\mathrm{cell}} = 3 \cdot 10^{-13}$ m^2/s in stratum corneum [2], i.e., the outermost layer of the skin was chosen as it resembles the cells used in the experiment most closely. Diffusion coefficient in cellular matrix D_{matrix} was obtained by fitting experimental data to R6G model data (see Section 4.2).

For the ring model, the same coefficient D_{matrix} was used, but diffusion coefficient in cells was adjusted taking into account that cells would not be fully squeezed into uniform cell ring and there would be some gaps at least between the sides of cells as shown in Fig. 1(c). In analyzed model, the formula for $D_{\mathrm{cell,\,ring}}$ was derived by calculating ratio between volume of sphere and cube:

$$D_{\mathrm{cell,\,ring}} = \frac{\pi}{6} D_{\mathrm{cell}} + \left(1 - \frac{\pi}{6}\right) D_{\mathrm{matrix}}.$$

WGA molecules diffuse only through cellular matrix with cells acting as immobilized barriers. Diffusion through porous media model was used to calculate diffusion coefficient [9, 19]:

$$D = (1 - \phi)^2 D_{\mathrm{matrix}},$$

where $(1 - \phi)$ accounts for porosity. It was demonstrated [17] that diffusion rates of R6G and WGA-Alexa488 dyes differ only by approximately 2.1% and the same R6G diffusion coefficient in matrix D_{matrix} was used.

Maximal concentration of binding sites per unit volume depends on a particular spheroid size and cell density. It was calculated using the formula

$$B_{\max} = \frac{N_{\mathrm{cell}}\, B_{\max,\,\mathrm{cell}}}{N_A\, V_{\mathrm{sphere}}}, \tag{10}$$

where $N_A = 6 \cdot 10^{23}$ is Avogadro number, $B_{\max,\,\mathrm{cell}} = 5 \cdot 10^5$ sites/cell is the number of binding sites in a single cell [8]. Binding rate constant (association constant) for WGA was determinant to vary from 10^2 to 10^6 in studies [3, 8, 16]. During computational experiment, several values of binding constant were used. These calculations showed that at rates $k_{\mathrm{bind}} = 10^3 - 10^4$ M^{-1}s^{-1}, reaction speed is maximal possible because the diffusion rate becomes a limiting factor. Therefore, $k_{\mathrm{bind}} = 10^3$ M^{-1}s^{-1} was chosen for other computations.

For the comparison with experimental data, accumulative concentration C_{acc} per volume, i.e., the total concentration in a spheroid divided by its volume, was calculated as an integral

$$C_{\mathrm{acc}}(t) = \frac{4\pi}{V_{\mathrm{sphere}}} \int_0^R C(t, r) r^2 \,\mathrm{d}r. \tag{11}$$

The presented equations (1)–(9) were solved numerically. First of all, 2D discrete grid was chosen consisting of 100 points in r direction and 240000 points in t direction.

Such a large number of points was necessary because modeling time $T = 24$ h was long and high accuracy had to be achieved. System of equations was discretized and solved numerically using finite difference method Crank–Nicolson implicit algorithm. Nonlinear system of algebraic equations was obtained and linearized by Picard iterative method. This linear system was then solved using Thomas algorithm. The iterative process was repeated until relative error between 2 iterations was no larger than $\varepsilon = 10^{-10}$. The process converged rapidly, and no more than 4 iterations were required. Necessary integrals such as (11) on discrete grid were calculated with 1st-order Newton–Cotes formula. All algorithms were implemented by the authors in Python with Numpy library.

4 Results

4.1 Analysis of experimental results

Accumulation of R6G in NIH3T3 spheroids was investigated using 2 methods: confocal microscopy and flow cytometry. It was shown that after 1 h of incubation, R6G accumulated only in the top layer of spheroid and the intensity of it was relatively low compared with the images after longer incubation times (Fig. 2(a)). Accumulation of R6G increased after longer incubation times. After 4 h of incubation, R6G fluorescence was observed through whole spheroid, and fluorescence intensity increased after 8 h and 24 h of incubation.

Accumulation of WGA-Alexa488 dye in NIH3T3 spheroids was demonstrated in Fig. 2(b). Penetration of WGA-Alexa488 dye in NIH3T3 cellular spheroid was slower than R6G dye. After 4 h, fluorescence of R6G dye was detected through the whole cellular spheroid optical section, while WGA-Alexa488 was detected only on the external part of the spheroid. Even after 24 h of incubation, only low fluorescence of WGA-Alexa488 was measured from internal parts of spheroid, suggesting that a small amount of WGA-Alexa488 molecules penetrated into the center of a cellular spheroid.

For quantitative evaluation of R6G accumulation in cellular spheroids, measurements with flow cytometry were made. Obtained results were demonstrated in Fig. 2(c) and used for the comparison with mathematical modeling results as presented in Fig. 3(a). Quantitative evaluation showed that after short times of incubations only cells, which were close to spheroid surface, had accumulated R6G, thus the mean fluorescence intensity was low. It was observed (Fig. 2(c), lower part) that fluorescence intensity was growing from 5 min to 4 h of incubation, but not as rapidly as the number of the cells, which had R6G inside (Fig. 2(c), upper part). After 2 h of incubation, $95 \pm 1\%$ of cells had accumulated R6G, but fluorescence intensity reached only $75 \pm 5\%$ of its maximum value. It can be concluded that some cells had accumulated only a small amount of R6G molecules. The peak of fluorescence intensity was observed after 4 h of incubation. Later, fluorescence intensity stabilized and did not change during measurements. This means that after 4 h of incubation with R6G, spheroids of radius $R \approx 150$ μm had fully accumulated R6G molecules. For comparison, in experiments with single layer of cells, maximum fluorescence intensity is reached after 2 h of incubation.

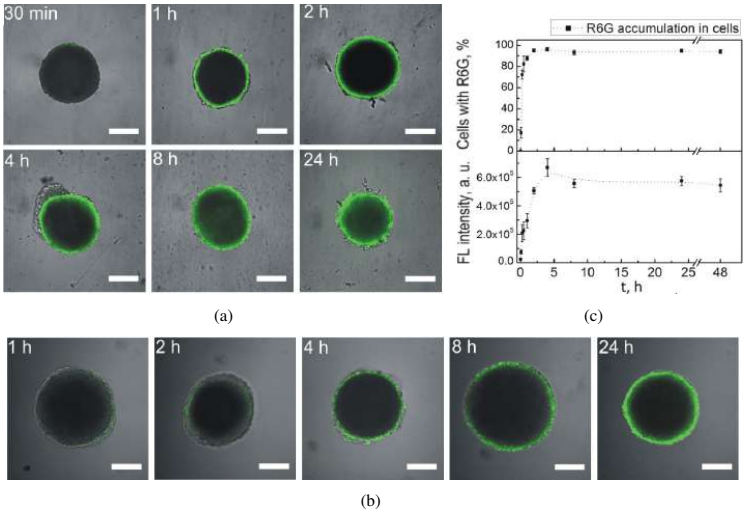

Figure 2. (a) Combined confocal microscopy and bright field images of R6G (green color, $\lambda_{\text{ex}} = 488$ nm) distribution in NIH3T3 cellular spheroids (8000 cells/drop, $R \approx 134$ μm), after different incubation times t. (b) Combined confocal microscopy and bright field images of WGA-Alexa488 (green color, $\lambda_{\text{ex}} = 488$ nm) distribution in NIH3T3 cellular spheroids, after different incubation times t. Representative images are shown. Scale bar 150 μm. (c) Quantitative evaluation of R6G accumulation in NIH3T3 spheroids. Percentage of cells with R6G molecules (upper) and florescence (FL) intensity per spheroid volume (lower) are presented in separate graphs. Every value is an average of 3 samples. Error bars represent standard deviation. Dotted line is an approximation.

4.2 Comparison between experimental and simulations data for R6G accumulation models

The diffusion coefficient in the cellular matrix was calculated by fitting model data to physical experimental data by least squares method. Accumulative R6G concentration, which was calculated using model (5)–(7) and integrated by (11), and fluorescence intensity from the experiment were normalized into nondimensionless values in order to compare them. Linear dependence between fluorescence intensity and concentration of the source is well known, and device constant can be calculated by normalizing, i.e., by dividing by maximal concentration and fluorescence intensity. It was determined that $D_{\text{matrix}} = 4.2 \cdot 10^{-13}$ m^2/s fits the experiment best (Fig. 3(a)) and device constant for this particular experiment is $6.4 \cdot 10^{10}$.

Another experimental data set was used for R6G model confirmation. Fluorescence intensities were calculated at 2 h time for spheroids with different radius and number of cells (Fig. 3(b)). Accumulated R6G concentrations were multiplied by device constant and plotted for comparison with experimental data (Fig. 3(b)). Intensities calculated per

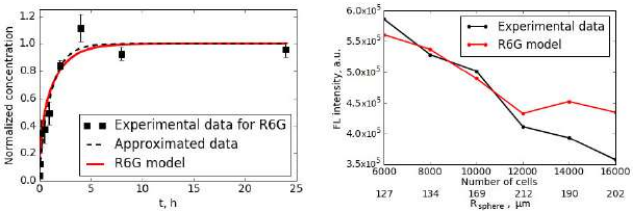

(a) (b)

Figure 3. (a) R6G model curve (red line) was fitted to experimental data (dashed line) in order to find diffusion coefficient in cellular matrix; 8000 cells, radius 134 μm. Black squares are experimental data and their standard deviation is represented by error bars. (b) Accumulated fluorescence intensity compared to intensities from experimental data; different spheroid size and number of cells, time $t = 2$ h.

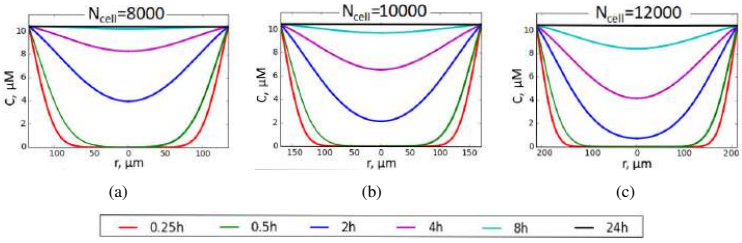

(a) (b) (c)

Figure 4. R6G concentration from center to the sides of spheroid at various time intervals and different spheroids: (a) $N_{\text{cells}} = 8000$, $R = 134$ μm; (b) $N_{\text{cells}} = 10000$, $R = 169$ μm; (c) $N_{\text{cells}} = 12000$, $R = 212$ μm.

cell are decreasing for larger spheroids, which are expected because it is increasingly difficult for the dye to reach inner layers. Very close correspondence between experiment and model was observed up until the largest numbers of cells. The size of cellular spheroid depends on initial cell number until the critical number of cells is reached. It was observed that, while growing spheroids from 6000 up to 10000 cells, the size of spheroid increased linearly, but spheroids with a large number of cells ($N_{\text{cell}} = 14000$ and $N_{\text{cell}} = 16000$) were similar in size and their radius did not depend on cell number. Thus our model showed that spheroids from 6000 up to 10000 cells are suitable for dyes penetration studies, whereas larger spheroids should not be used because of inaccuracies.

Using the R6G migration model (Section 3.2), R6G dye accumulation inside spheroid was calculated. Figure 4 shows R6G concentration dependency from distance r to the center at various time intervals. Three spheroids were modeled with a different number of cells, i.e., cell/matrix density and spheroid radius R. These parameters were taken from experimental data.

It can be observed that the first few layers ($\sim 20{-}30$ μm) were almost fully accumulated after about 15 min in all spheroids. The center of the smallest analyzed spheroid

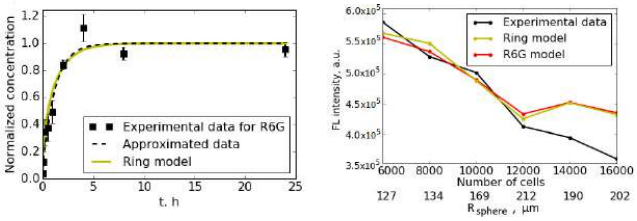

(a) (b)

Figure 5. (a) Ring model results compared with spheroid penetration by time. Diffusion coefficients are taken from R6G model. Spheroid with 8000 cells, radius 134 μm. (b) Accumulated fluorescence intensity from ring model data, R6G model and experiment, time $t = 2$ h.

was filled after less than 8 h (Fig. 4(a)), but the center of the larger spheroid in Fig. 4(c) was reached much slower. After 24 h, all spheroids were completely filled with R6G molecules.

An alternative ring model was proposed in order to better understand R6G penetration into spheroids as explained in Section 3.3. Penetration curve in Fig. 5(a) was calculated with R6G cell and matrix diffusion coefficients, which were used in the previously analyzed R6G model. The curve is very close to approximated experimental data as mean squared error is only 0.04%. For comparison, penetration curve calculated with R6G model (Fig. 3(a)) has error of 0.05% from experimental data. It can be concluded that error is very small in both cases.

In Fig. 5(b), fluorescence intensity of the ring model was plotted against experimental and R6G model data. While both models agree fairly well with experimental data, ring model is slightly more accurate with 4.9% error compared to 5.2% error for R6G model. From these results we conclude that both models are successful and can be used for further analysis of dyes penetration. Ring model can be applied at determining the effects of cells diameter and cellular matrix layer size, i.e., the average distance between cells, on dye penetration properties.

4.3 Nonlinear WGA model analysis

WGA model was proposed in Section 3.1 to analyze WGA molecules diffusion and binding to cells. This process is experimentally difficult to conduct and modeling has to be employed. It is expected that the WGA model would be accurate because WGA diffusion in 3D spheroids is closely related to R6G diffusion, which agrees with the experiment well as shown in Section 4.2. Comparing with R6G model, reaction term was added to account for binding to cells, and binding rate k_{bind} and concentration of binding sites $B_{\max}$ was evaluated. Diffusion was calculated only in the cellular matrix because WGA molecules do not diffuse through the cell membrane.

Using WGA model, concentration in cellular matrix C_{out} and concentration of bound WGA molecules C_{bind} were computed and shown in Fig. 6 upper and middle rows for

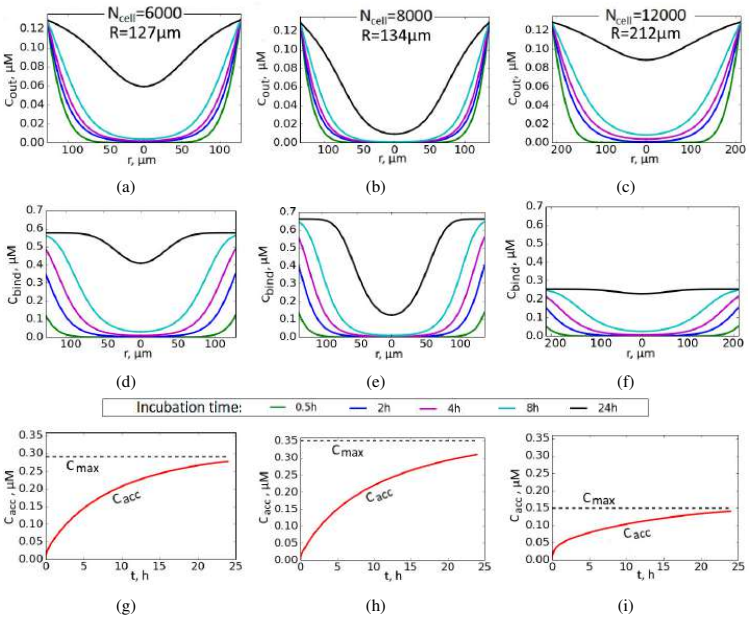

Figure 6. WGA dye concentration C_{out} in cellular matrix (upper row) and C_{bind} in cells (middle row). Bottom row: accumulative WGA concentration C_{acc} in matrix and cell together. $C_{\max}$ shows maximum concentration for each spheroid. Left column: spheroid with 6000 cells and radius 127 μm, middle column: spheroid with 8000 cells and radius 134 μm, right column: spheroid with 12000 cells and radius 212 μm.

3 different spheroids. It was observed that the penetration rate for the smaller spheroid (Fig. 6(a)) was faster than for the larger one (Fig. 6(b)). Spheroid formed from 8000 cells was denser than 6000 cells spheroid, and thus there was a greater amount of binding sites (compare Fig. 6(e) with Fig. 6(d)). Because of that, WGA penetration into the center of 8000 cell spheroid was slowed down not only by greater size but also by faster binding process.

In case of largest spheroids (Fig. 6(c)), it was observed in the experiment that they were much sparser (see x-axis in Fig. 3(b)). As it was mentioned before, some changes in spheroid formation occurred due to a large number of cells, and it was demonstrated in our previous experiment that spheroids porosity depends on size and cells type [14]. 3D spheroids formed from cancer cells are sparser because cancer cells tend to migrate and metastize. As shown in Fig. 6(f), the number of binding sites per unit volume was much smaller, and almost all sites were taken in 24 h. Therefore, diffusion was not slowed so much by reaction term, and spheroid center was almost completely penetrated by WGA in 24 h even though the spheroid was larger than 6000 and 8000 cells spheroids.

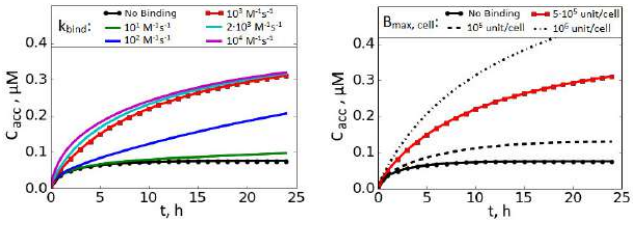

(a) (b)

Figure 7. Accumulative WGA concentration in both cells and cellular matrix with: (a) different binding constant k_{bind} and fixed $B_{\mathrm{max,\,cell}} = 5 \cdot 10^{-5}$ unit/cell binding sites; (b) different number of binding sites $B_{\mathrm{max,\,cell}}$ and fixed $k_{\mathrm{bind}} = 10^3\ \mathrm{M}^{-1}\mathrm{s}^{-1}$. Red line marks results with same binding parameters. Spheroid formed from 8000 cells and radius 134 μm was used.

These nonlinear effects were further explained in Figs. 6(g), (h), (i). Accumulated concentration per volume

$$C_{\mathrm{acc}}(t) = (1-\phi)\, C_{\mathrm{out,\,acc}}(t) + \phi\, C_{\mathrm{bind,\,acc}}(t), \quad \phi = \frac{N_{\mathrm{cell}}\, V_{\mathrm{cell}}}{V_{\mathrm{sphere}}},$$

was calculated and compared with maximum concentration per volume

$$C_{\max} = (1-\phi)\, C_{\mathrm{outside}} + \phi\, B_{\max},$$

which can accumulate into cellular matrix and cell membranes of spheroids. Accumulated concentrations in matrix $C_{\mathrm{out,\,acc}}$ and in cells $C_{\mathrm{bind,\,acc}}$ were calculated by (11). 8000 cell spheroid (Fig. 6(h)) was the densest, and therefore, it accumulated more WGA molecules on average than the smaller spheroid (Fig. 6(g)). It was observed that the accumulative concentration of 8000 cell spheroid was greater even though the center was almost not incubated at all at 24 h. It can be explained by spherical geometry – outer layers of a sphere accounts for a much greater volume than inner layers. On the other hand, for 12000 cell, spheroid $C_{\max}$ and C_{acc} are much smaller due to lesser dense ($B_{\max}$ is 2–3 times smaller than $B_{\max}$ for 6000 and 8000 cells spheroids), and its matrix layer was penetrated more rapidly (Fig. 6(c)) than for smaller spheroids.

The effect of reaction parameters to accumulative WGA dye concentration was investigated for spheroid of radius 134 μm and formed from 8000 cells. Various values (Fig. 7(a)) of binding constant k_{bind} were tested. It was observed that with $k_{\mathrm{bind}} = 10^4\ \mathrm{M}^{-1}\mathrm{s}^{-1}$ accumulation speed no longer increased, which means that diffusion process is a limiting factor and this binding rate is so rapid that all available dye molecules bind almost instantly. However, at lower binding rations ($< 10^2\ \mathrm{M}^{-1}\mathrm{s}^{-1}$), accumulation speed was almost linear. Then the constant was set to zero, the binding process stopped, and concentration reached its balance at about 4 h, which is compatible with R6G models.

In Fig. 7(b), the effects of the number of binding sites per cell $B_{\mathrm{max,\,cell}}$, which was used to calculate binding site concentration $B_{\max}$ by (10), can be seen. As expected, a greater number of sites resulted in increased accumulative concentration. Figures 7(a),

(b) showed that WGA dye accumulation dynamics strongly depend on binding constant and number of receptors (binding sites) in the cells. From modeling results at fixed binding rate constant $k_{\mathrm{bind}} = 10^3\ \mathrm{M}^{-1}\mathrm{s}^{-1}$ it could be predicted that 3.4 times more WGA dye molecules accumulated after 24 hour for cells with 10 times more receptors on their plasma membranes.

5 Conclusions

In this study, accumulation and distribution of both R6G and WGA-Alexa488 fluorescent dyes in NIH3T3 cellular spheroids was demonstrated with confocal microscopy images. After 30 min of incubation, R6G dye accumulated only in the top layer of the cellular spheroid, whereas after 4 h of incubation, fluorescence of R6G was seen through the whole spheroid. In comparison, after 4 h of incubation with WGA-Alexa488, only spheroid surface was stained. Additionally, quantification of R6G dye uptake in NIH3T3 spheroid was evaluated using flow cytometry. The peak of fluorescence intensity had been observed after 4 h incubation, and after longer incubation times, the dynamic balance of R6G molecules in cells was established.

Diffusion–reaction equation model was presented for analysis of dyes penetration into cellular spheroids. Both cases of the model for R6G dye, i.e., linear diffusion model and ring model, showed a close correspondence with experimental results. Using the model, it was calculated that the diffusion coefficient in the cellular matrix is $D = 4.2 \cdot 10^{-13}\ \mathrm{m}^2/\mathrm{s}$, which is about 4 times higher than the diffusion coefficient in cells used in calculations. Accumulation dynamics were analyzed, and it was shown that about 4 h are necessary to reach a balance, but the center zone is not fully incubated until about 10 h. These dynamics also strongly depend on the spheroid size and density.

Dynamics of WGA-Alexa488 dye penetration into spheroid were analyzed using nonlinear case of the model. The effect of binding rate and binding sites number to penetration dynamics was researched. Our experimental and modeling results showed that dynamic of WGA-Alexa488 dye accumulation in cells is nonlinear because of several biological processes such as rate of endocytosis, the density of cells and extracellular matrix, type and concentration of receptors in the cells plasma membrane, and other factors.

References

1. T.-M. Achilli, S. McCalla, J. Meyer, A. Tripathi, J.R. Morgan, Multilayer spheroids to quantify drug uptake and diffusion in 3D, *Mol. Pharm.*, **11**(7):2071–2081, 2014.
2. Yu.G. Anissimov, X. Zhao, M.S. Roberts, A.V. Zvyagin, Fluorescence recovery after photobleaching as a method to determine local diffusion coefficient in the stratum corneum, *Int. J. Pharm.*, **435**(1):93–97, 2012.
3. G. Bains, R.T. Lee, Y.C. Lee, E. Freire, Microcalorimetric study of wheat germ agglutinin binding to N-acetylglucosamine and its oligomers, *Biochemistry*, **31**(50):12624–12628, 1992.
4. G. Cernansky, D.-F. Liau, S.A. Hashim, S.F. Ryan, Estimation of phosphatidylglycerol in fluids containing pulmonary surfactant., *J. Lipid Res.*, **21**(8):1128–1131, 1980.

5. P.L. Chariou, K.L. Lee, J.K. Pokorski, G.M. Saidel, N.F. Steinmetz, Diffusion and uptake of tobacco mosaic virus as therapeutic carrier in tumor tissue: Effect of nanoparticle aspect ratio, *J. Phys. Chem. B*, **120**(26):6120–6129, 2016.
6. Yu. Chenyakin, D.A. Ullmann, E. Evoy, L. Renbaum-Wolff, S. Kamal, A.K Bertram, Diffusion coefficients of organic molecules in sucrose–water solutions and comparison with Stokes–Einstein predictions, *Atmos. Chem. Phys.*, **17**(3):2423–2435, 2017.
7. J.C. Dittmer, R.L. Lester, A simple, specific spray for the detection of phospholipids on thin-layer chromatograms, *J. Lipid Res.*, **5**(1):126–127, 1964.
8. P. Ganguly, N.G. Fossett, The role of sialic acid in the activation of platelets by wheat germ agglutinin, *Blood*, **63**(1):181–187, 1984.
9. Y. Gao, M. Li, B. Chen, Z. Shen, P. Guo, M.G. Wientjes, J. L.-S. Au, Predictive models of diffusive nanoparticle transport in 3-dimensional tumor cell spheroids, *AAPS J.*, **15**(3):816–831, 2013.
10. P.-O. Gendron, F. Avaltroni, K.J. Wilkinson, Diffusion coefficients of several rhodamine derivatives as determined by pulsed field gradient–nuclear magnetic resonance and fluorescence correlation spectroscopy, *J. Fluoresc.*, **18**(6):1093, 2008.
11. T.T. Goodman, J. Chen, K. Matveev, S.H. Pun, Spatio-temporal modeling of nanoparticle delivery to multicellular tumor spheroids, *Biotechnol. Bioeng.*, **101**(2):388–399, 2008.
12. C.P. Graff, K.D. Wittrup, Theoretical analysis of antibody targeting of tumor spheroids: Importance of dosage for penetration, and affinity for retention, *Cancer Res.*, **63**(6):1288–1296, 2003.
13. D.R. Grimes, C. Kelly, K. Bloch, M. Partridge, A method for estimating the oxygen consumption rate in multicellular tumour spheroids, *J. R. Soc. Interface*, **11**(92):20131124, 2014.
14. G. Jarockyte, D. Dapkute, V. Karabanovas, J.V. Daugmaudis, F. Ivanauskas, R. Rotomskis, 3D cellular spheroids as tools for understanding carboxylated quantum dot behavior in tumors, *Biochim. Biophys. Acta, Gen. Subj.*, **1862**(4):914–923, 2018.
15. Y. Masuda, T. Oguma, Examination of intrahepatic flow distribution by vital staining with rhodamine 6G in isolated perfused rat liver, *Jpn. J. Pharmacol.*, **83**(3):215–224, 2000.
16. Y. Nagata, M.M. Burger, Wheat germ agglutinin molecular characteristics and specificity for sugar binding, *J. Biol. Chem.*, **249**(10):3116–3122, 1974.
17. Z. Petrášek, P. Schwille, Precise measurement of diffusion coefficients using scanning fluorescence correlation spectroscopy, *Biophys. J.*, **94**(4):1437–1448, 2008.
18. C. Saengkhae, C. Loetchutinat, A. Garnier-Suillerot, Kinetic analysis of rhodamines efflux mediated by the multidrug resistance protein (MRP1), *Biophys. J.*, **85**(3):2006–2014, 2003.
19. B.A. Westrin, A. Axelsson, Diffusion in gels containing immobilized cells: A critical review, *Biotechnol. Bioeng.*, **38**(5):439–446, 1991.
20. C.S. Wright, Structural comparison of the two distinct sugar binding sites in wheat germ agglutinin isolectin II, *J. Mol. Biol.*, **178**(1):91–104, 1984.

Rokas Astrauskas

Computer Modelling of Reaction-Diffusion Processes in Scanning Electrochemical Microscopy and in Cell Spheroids

Doctoral Dissertation
Natural Sciences
Informatics (N 009)
Thesis Editor: ...

Reakcijos-difuzijos procesų kompiuterinis modeliavimas skenuojančioje mikroskopijoje ir ląstelių sferoiduose

Daktaro disertacija
Gamtos mokslai
Informatika (N 009)
Santraukos redaktorė: ...

Vilnius University Press
9 Saulėtekio Ave., Building III, LT-10222 Vilnius
Email: info@leidykla.vu.lt, www.leidykla.vu.lt
Print run of ... copies